AGU PUBLICATIONS

Geophysical Research Letters

RESEARCH LETTER
10.1002/2016GL068393

Key Points:
- LDEX observes lunar exospheric pickup ions through integrator channel at high time/spatial resolution
- Ion production scale height of 100 km, peak near 0800 LT, and linear dependence on solar wind flux
- Comparison to model suggests Ar^+ and CO^+ as dominant ion species, with possible contribution from Al^+

Correspondence to:
A. R. Poppe,
poppe@ssl.berkeley.edu

Citation:
Poppe, A. R., J. S. Halekas, J. R. Szalay, M. Horányi, Z. Levin, and S. Kempf (2016), LADEE/LDEX observations of lunar pickup ion distribution and variability, *Geophys. Res. Lett.*, *43*, doi:10.1002/2016GL068393.

Received 24 FEB 2016
Accepted 17 MAR 2016
Accepted article online 22 MAR 2016

LADEE/LDEX observations of lunar pickup ion distribution and variability

A. R. Poppe[1,2], J. S. Halekas[2,3], J. R. Szalay[4], M. Horányi[2,5], Z. Levin[5], and S. Kempf[2,5]

[1]Space Sciences Laboratory, University of California, Berkeley, California, USA, [2]Solar System Exploration Research Virtual Institute, NASA Ames Research Center, Moffett Field, California, USA, [3]Department of Physics and Astronomy, University of Iowa, Iowa City, Iowa, USA, [4]Southwest Research Institute, San Antonio, Texas, USA, [5]Laboratory for Atmospheric and Space Physics and Department of Physics, University of Colorado Boulder, Boulder, Colorado, USA

Abstract We report fortuitous observations of low-energy lunar pickup ion fluxes near the Moon while in the solar wind by the Lunar Dust Experiment (LDEX) on board the Lunar Atmosphere and Dust Environment Explorer (LADEE). We describe the method of observation and the empirical calibration of the instrument for ion observations. LDEX observes several trends in the exospheric ion production rate, including a scale height of approximately 100 km, a positive, linear correlation with solar wind flux, and evidence of a slight enhancement near 7–8 h local time. We compare the LDEX observations to both LADEE Neutral Mass Spectrometer ion mode observations and theoretical models. The LDEX data are best fit by total exospheric ion production rates of $\approx 6 \times 10^3$ m^{-3} s^{-1} with dominant contributions from Al^+, CO^+, and Ar^+, although the LDEX data suggest that the aluminum neutral density and corresponding ion production rate are lower than predicted by recent models.

1. Introduction

The surface-bound exosphere of the Moon is composed of many distinct species reflecting several different production mechanisms. These mechanisms include radiogenic outgassing, sputtering by and neutralization of incident charged particles (i.e., solar wind protons and alphas), micrometeorite impact vaporization, and photon-stimulated desorption [*Stern*, 1999; *Yakshinskiy and Madey*, 1999; *Sarantos et al.*, 2012a; *Vorburger et al.*, 2014]. Despite several decades of observational searches, an inventory and full understanding of the various neutral exospheric species at the Moon is not yet complete. To address this, the Lunar Atmosphere and Dust Environment Explorer (LADEE) completed 6 months of in situ and remote sensing observations of the neutral lunar exosphere [*Elphic et al.*, 2014], with confirmed detections of neutral helium, neon, argon, sodium, potassium, and several ionized species [*Benna et al.*, 2015; *Halekas et al.*, 2015; *Hurley et al.*, 2016; *Colaprete et al.*, 2016; *Hodges and Mahaffy*, 2016].

In addition to measuring neutral species, observations of pickup ions provide a powerful method to probe the composition and structure of both the lunar exosphere and surface [e.g., *Hartle and Killen*, 2006]. Lunar pickup ions have been detected by several missions including Active Magnetospheric Particle Tracer Explorers [*Hilchenbach et al.*, 1993], Wind [*Mall et al.*, 1998], Kaguya [*Yokota et al.*, 2009; *Tanaka et al.*, 2009], and Acceleration, Reconnection, Turbulence and Electrodynamics of the Moon's Interaction with the Sun (ARTEMIS) [*Halekas et al.*, 2012a; *Poppe et al.*, 2012]. The reported compositions of these ions have spanned masses 2 amu to 56 amu, including He^+, C^+, O^+, Na^+, Al^+, Si^+, K^+, Ar^+, and Fe^+. More recently, the LADEE Neutral Mass Spectrometer (NMS) has reported observations of lunar exospheric ions of masses 2 (H_2^+), 4 (He^+), 12 (C^+), 16 (O^+), 20 (Ne^+), 23 (Na^+), 28 ($Si^+/CO^+/N_2^+$), 39 (K^+), and 40 (Ar^+) amu [*Halekas et al.*, 2015]. In addition to the LADEE/NMS, which has a dedicated ion mass spectrometry mode [*Mahaffy et al.*, 2014], it was discovered while in lunar orbit that a specific observing mode of the Lunar Dust Experiment (LDEX) on board LADEE, primarily designed to detect submicron dust grains, is also sensitive to the net current of low-energy pickup ions from the lunar exosphere [*Horányi et al.*, 2014; *Szalay and Horányi*, 2015]. Due to its large geometric factor and near-continuous operation during the 6 month LADEE mission, the LDEX current data set affords a powerful opportunity for studying the total lunar pickup ion current and its variability with respect to several key parameters, including local time, altitude, and solar wind flux. In turn, these correlations provide information about the structure and variability of the Moon's neutral exosphere.

In this paper, we report fortuitous observations of pickup ion fluxes at the Moon by LDEX on board the LADEE spacecraft. In section 2, we describe the LDEX instrument and present a representative set of LDEX current observations and their interpretation as lunar exospheric ions. In section 3, we aggregate and present the pickup ion current with respect to mission time, altitude, solar wind flux, and local lunar time. Finally, we discuss these results and compare to LADEE/NMS observations and an exospheric model in section 4 and conclude in section 5.

2. LDEX Observations

LDEX is an impact ionization dust detector designed to measure the size and spatial distributions of both >0.3 μm and <0.3 μm grains using separate methods while in orbit around the Moon [*Horányi et al.*, 2014]. For grains with radii > 0.3 μm, individual impact ionization events are detected and the resulting charge is translated into grain mass using empirically determined calibration curves. For grains with radii < 0.3 μm, the charge generated upon impact is individually smaller than the LDEX detection threshold (≈ 3000 electrons), yet the net current arising from multiple impacts can yield information about the net flux of < 0.3 μm grains. This latter mode, referred to as the "integrator" (see full description in *Szalay and Horányi* [2015]), also yields an additional, serendipitous measurement of low-energy ambient ions, presumably originating from the lunar exosphere.

Figure 1 shows four consecutive orbits (#603–606) of LDEX current observations and concurrent ARTEMIS data from 4 to 5 December 2013. Figure 1a shows the interplanetary convection electric field as observed by the ARTEMIS spacecraft in Solar Selenocentric Ecliptic coordinates; Figure 1b shows the negative of the dot product between the interplanetary convection electric field and the LDEX boresight, $-\hat{E}_c \cdot \hat{b}$; Figure 1c shows the current observed by LDEX (black) and the angle between the electric field and the LDEX boresight vector, $\arccos(-\hat{E}_c \cdot \hat{b})$ (blue); and Figure 1d displays the LADEE spacecraft solar zenith angle. Finally, the two colored bars at the bottom of Figure 1 denote the sunlit/shadowed periods of the LADEE/LDEX orbit (red is sunlit and black is eclipse) and the periods of LDEX operation (green). Field-to-boresight dot product values greater than 0 indicate an electric field pointing into the instrument, allowing detection of exospheric ions, while values less than 0 indicate an electric field pointing away from the LDEX instrument; thus, no exospheric ions should be observable during these periods. Over this approximately 8h interval, the convection electric field is highly variable, reflecting changes in the interplanetary magnetic field. In turn, the electric field-to-boresight vector rapidly changes, in addition to a longer period variation due to LDEX's evolving boresight direction as LADEE orbits the Moon.

On the first three orbits shown, #603, 604, and 605, LDEX observes variable currents between approximately 0.2×10^6 and 1.5×10^6 ions s^{-1} on the sunlit side of the Moon. On orbit #606, LDEX observes a nearly constant current of 0.2×10^6 ions s^{-1} during the majority of the sunlit portion of the orbit. During the eclipse portion of all orbits, currents drop to approximately 0 before increasing slightly near the end of each eclipse period before reentering sunlight. For the sunlit portions of the first three orbits, the convection electric field, Figure 1b, is oriented for most of the time such that the newly born exospheric ions will be accelerated along trajectories that enter the LDEX instrument, i.e., $-\hat{E}_c \cdot \hat{b} > 0$ in Figure 1b and $\arccos(-\hat{E}_c \cdot \hat{b}) > 0$ in Figure 1c. Several correlations can be seen between the LDEX current and the electric field-to-boresight vector. For example, at 17:24 UT during orbit #603, a sharp decrease in the E_z component changes the field-to-boresight dot product from +0.3 to +0.9, while the LDEX current jumps sharply from 0.3×10^6 to 1.0×10^6 ions s^{-1}. This is followed by a concurrent, gradual decrease in both the current and dot product up until LADEE enters the lunar shadow. Also, at 21:15 UT during orbit #605, both the E_y and E_z components undergo a sharp rotation, changing the field-to-boresight dot product from nearly +1.0 to −0.3. Concurrently, the LDEX current drops from approximately 1.3×10^6 to 0.2×10^6 ions s^{-1}. In comparison, during orbit #606 the electric field is pointing away from the LDEX boresight, $-\hat{E}_c \cdot \hat{b} < 0$ (see Figure 1b), for times when LDEX is operating in sunlight. The current measured here by LDEX of approximately 0.2×10^6 ions s^{-1} is a background source that cannot originate from low-energy exospheric ions.

Since the LDEX instrument was not originally designed to measure ambient ions, the efficiency and calibration of the instrument with respect to the incoming pickup ion energy and angle is not a priori known and must be determined empirically. Figure 2a shows all LDEX current data on the dayside of the Moon and in the solar wind as a function of the dot product between the LDEX boresight and the convection electric field. The median current, shown in red, is constant at approximately 3×10^5 ions s^{-1} for $-\hat{E}_c \cdot \hat{b} < 0$ and

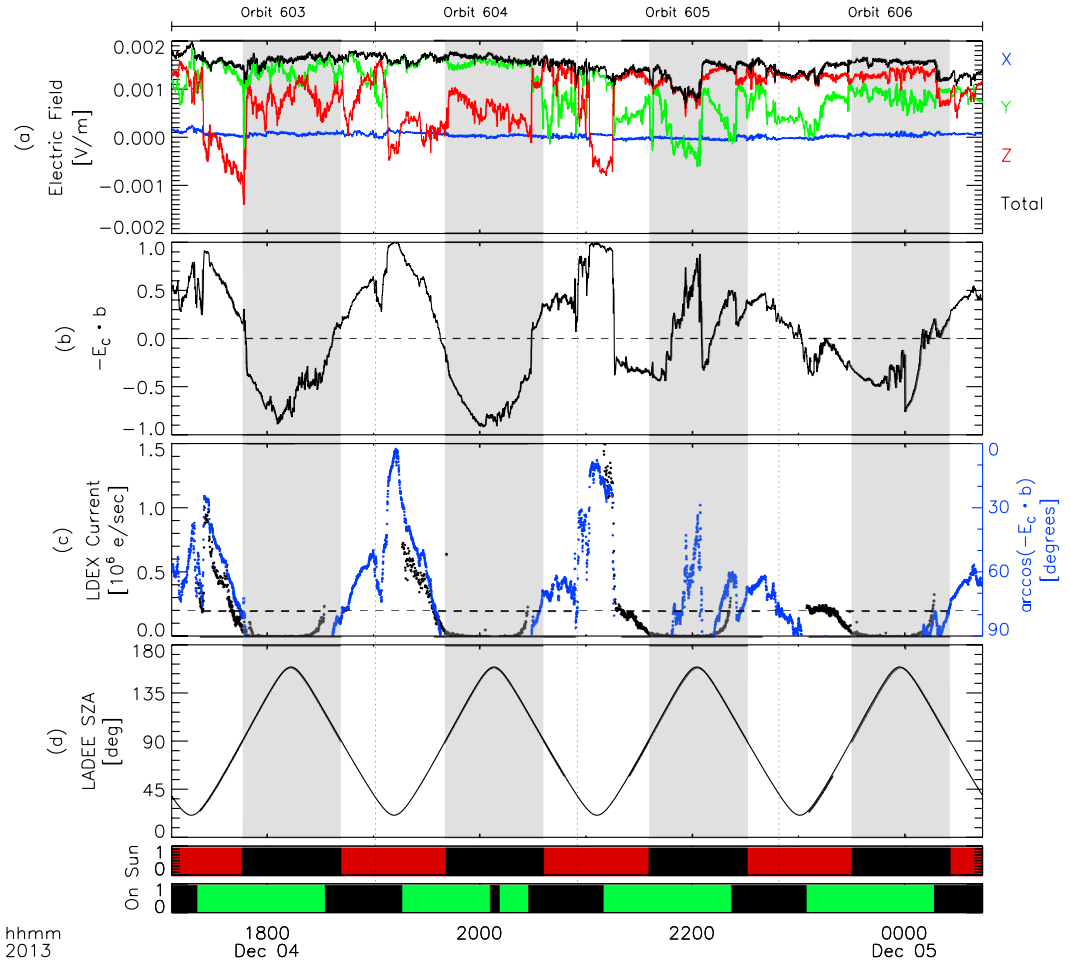

Figure 1. LDEX observations of lunar exospheric current and associated ARTEMIS data for four orbits on 4–5 December 2013. (a) The convection electric field as observed by ARTEMIS, (b) the negative dot product between the electric field vector and the LDEX boresight, (c) the observed LDEX current (black) and the angle between the electric field and LDEX boresight (blue), and (d) the LADEE solar zenith angle about the Moon. The two color bars at the bottom show (i) the sunlit (red) and shadowed (black) periods at the LADEE spacecraft and (ii) the times of operation of the LDEX instrument (green). The horizontal dashed line in Figure 1c denotes the LDEX background current level (see text for full discussion). Individual orbit numbers are denoted at the very top of the plot. Vertical gray shaded regions denote periods where the LADEE spacecraft was in the lunar optical shadow.

increases steadily as a function of dot product for $-\hat{E}_c \cdot \hat{b} > 0$. The current measured for $-\hat{E}_c \cdot \hat{b} < 0$, i.e., when LDEX cannot measure pickup ions, is linearly correlated with solar wind flux as shown in Figure 2b. One plausible explanation for this background signal is energetic neutral atoms (hydrogen, specifically) originating from solar wind protons that are neutralized and reflected upon striking the lunar surface [e.g., *Wieser et al.*, 2009; *Rodríguez et al.*, 2012]. After reflection, these energetic neutral atoms travel into LDEX regardless of the interplanetary convection electric field direction and presumably sputter ions or re-ionize upon impacting the LDEX target, thus generating a current independent of the electric field direction and directly correlated with solar wind flux [*Walker et al.*, 2015]. While we cannot fully confirm this theory, we use Figure 2b and the solar wind flux observed by ARTEMIS to appropriately subtract the background signal from the total LDEX current and obtain the current due only to low-energy exospheric pickup ions. Figure 2c shows the median background-subtracted LDEX current as a function of the angle between the LDEX boresight and the convection electric field. With the background subtraction in place, the median LDEX current (black) matches well with a fit of the form $f(\theta) = \exp(-\theta^2/2\theta_o^2)$, where $\theta_o = 30°$, shown in red. This function encompasses not only the acceptance area of the LDEX boresight (i.e., proportional to $\cos\theta$) but also the unknown detection efficiency for low-energy ions entering the LDEX electrostatic fields as a function of θ. This function also

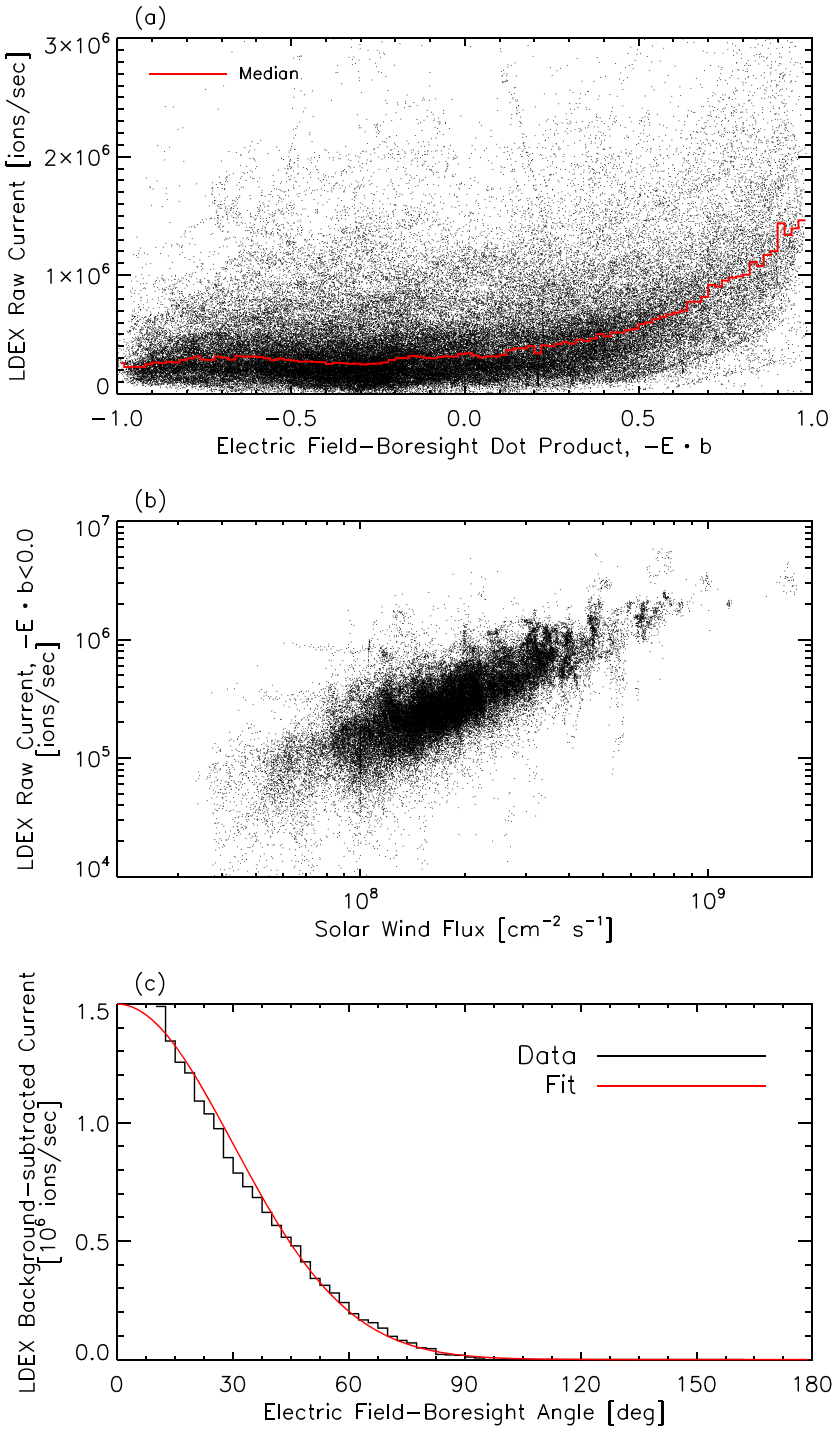

Figure 2. (a) The raw LDEX current versus the dot product between the electric field vector and instrument boresight for all times on the lunar dayside and in the solar wind. (b) The raw LDEX current for times when the electric field points away from the LDEX boresight versus the solar wind flux. (c) The median background-subtracted LDEX current (black) and fit (red) versus the angle between the electric field vector and instrument boresight.

averages over the relative efficiency of LDEX to varying pickup ion mass; however, since the mass distribution of the incoming flux is a priori unknown, such an approximation is unavoidable. Importantly, we also note that the fit shown in Figure 2c only characterizes the relative angular sensitivity of LDEX for low-energy ions and does not provide an absolute calibration for the instrument. Thus, without further ground calibration experiments using the spare LDEX instrument, we are limited to presenting the observed, background-subtracted current in relative, rather than absolute, terms.

We note that while the ionization and acceleration of lunar exospheric pickup ions is the most plausible explanation for the behavior of the LDEX current as shown in Figure 2, there are other possibilities that we must consider. While low-energy ($<\approx$ 100 eV) pickup ions will be electrostatically focused into the LDEX multichannel plate detector and recorded as a current, higher-energy pickup ions will pass through the electrostatic fields and strike the hemispherical LDEX detector. These pickup ions will presumably sputter the detector, generating additional neutral and ionized rhodium atoms, which will also contribute to the measured current. This additional signal should have the same dependence on the direction of the convection electric field as the low-energy pickup ions. Additionally, solar wind protons are known to reflect from both the lunar surface and lunar crustal magnetic anomalies [e.g., *Saito et al.*, 2008; *Lue et al.*, 2011; *Halekas et al.*, 2013]; however, due to the scattered nature of the proton trajectories with respect to the convection electric field, we expect that any current from low-energy protons entering LDEX will be uncorrelated with the electric field direction and, thus, subtracted out as background signal via the process described above.

3. Analysis

The LDEX instrument recorded the ambient exospheric pickup ion current through its integrator channel over 176 days from 23 October 2013 to 18 April 2014. We restricted our analysis to times when (a) the Moon was in the solar wind as determined from the ARTEMIS data, (b) LDEX was on the dawn hemisphere of the lunar dayside, (c) the convection electric field magnitude satisfied $|\vec{E}| > 10^{-3}$ V/m, and (d) the convection electric field satisfied $\vec{E} \cdot \hat{r} < 0$, where $\hat{r}$ is the LADEE position vector in lunar centered coordinates. Constraint (c) on $|\vec{E}|$ restricts observations to those times when the observable column length of newly born pickup ions is a small fraction of a lunar radius, thus ensuring a local measurement, and constraint (d) ensures that LDEX is observing only pickup ions from the exosphere and not also those ions sputtered directly from the surface [i.e., *Elphic et al.*, 1991]. A determination of the flux of directly sputtered surface ions is an important investigation [see *Sarantos et al.*, 2012b] yet left for future work due to complications separating the exospheric and surface ion currents.

At each time satisfying these constraints, we explore the dependence of the background-subtracted, relative ion production rate with several relevant parameters. Figure 3a shows the relative ion production rate as a function of LADEE mission time for both individual LDEX observations (black dots) and a 2 day binned median (red bars). Periodic gaps every ≈28 days are terrestrial magnetotail crossings. Within the approximately 6 month time frame explored by LADEE, we see no significant evidence of longer-term (i.e., weekly to monthly) temporal variations, although we do note increased variability in the early months of the mission, most likely due to reduced observational time and lower statistical sampling. Figure 3b shows ion volume production rate $R(z)$, where z is the altitude above the lunar surface. LADEE's orbit during its primary mission spanned $10 < z < 100$ km with a limited number of observations either above 100 km or below 10 km. LDEX observed a slowly decreasing ion volume production rate between 10 and 100 km with a scale height of approximately 100 km. We caution that the altitude bins above 90 km suffer from poor measurement statistics and are most likely highly uncertain. Figure 3c shows the ion volume production rate as a function of the incoming solar wind flux as measured concurrently by the ARTEMIS spacecraft. For solar wind fluxes less than approximately 10^8 cm^{-2} s^{-1} the production rate is roughly constant, while for solar wind fluxes greater than 10^8 cm^{-2} s^{-1}, the production rate increases in linear correlation with the solar wind flux. Finally, the variation of ion volume production rate as a function of lunar local time is shown in Figure 3d. Due to operational constraints, the majority of LDEX observations were taken between 6:00 and 11:00 LT; thus, despite the presence of some measurements at times past 11:00 LT, we restrict our analysis to times before 11:00 LT. While the ion volume production rate is relatively flat between 06:00 and 11:00 LT, there is some evidence of a local maximum near approximately 07–08 LT.

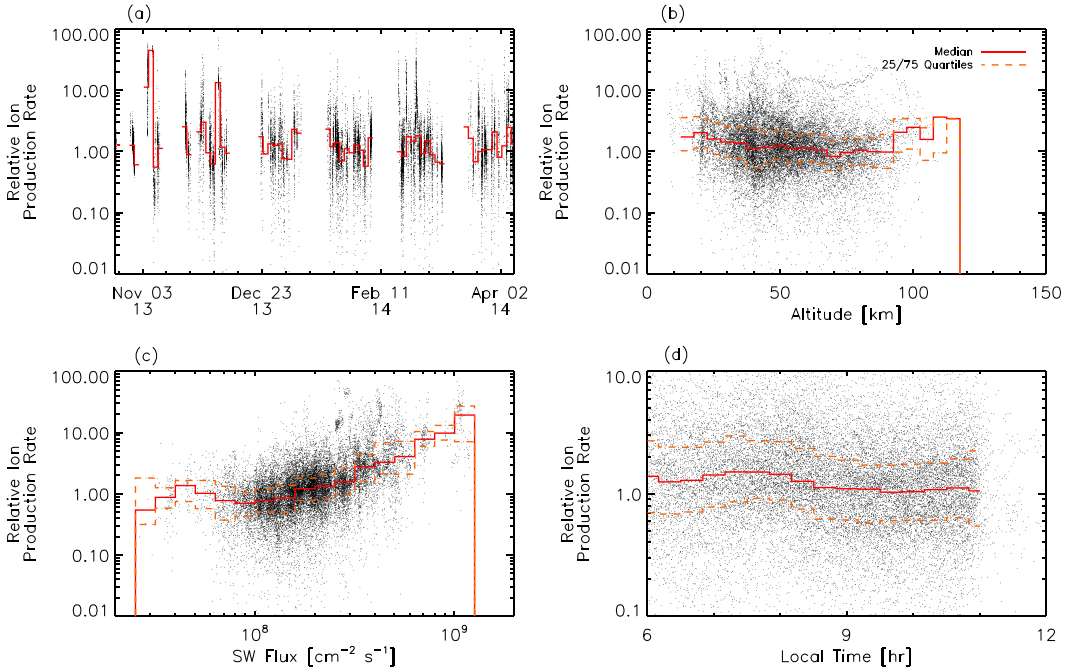

Figure 3. Relative lunar exospheric ion volume production rates as a function of (a) time throughout the LADEE mission, (b) altitude, (c) solar wind flux, and (d) local time around the Moon. The solid red and dashed orange lines denote the median and 25/75% quartiles, respectively. Note that in Figure 3d we have plotted a smaller range in ion production rate to better depict the relative variations in local time.

4. Discussion

In order to place the LDEX observations into context, we compare the data to calculations of lunar exospheric ion production rates. Where possible, we use in situ measurements of either neutral densities (multiplied by associated ionization rates) or ion production rates; however, in cases where measurements of a given species are not available, we use modeled neutral densities (again, along with relevant ionization rates). For He, Ne, and Ar, we use LADEE/NMS neutral density measurements [*Benna et al.*, 2015], for C, O, and CO we use the observations from LADEE/NMS ion mode [*Halekas et al.*, 2015], and for the remaining species (Na, Mg, Al, Si, K, Ca, Ti, and Fe) we use the model of *Sarantos et al.* [2012a]. Na and K are modeled as products from photon-stimulated desorption, which dominates over the sputtered and impact vaporization contributions, with a neutral temperature of 1200 K [*Yakshinskiy and Madey*, 1999, 2004]. The refractory species (C, O, Na, Mg, Al, Si, K, Ca, Ti, and Fe) are modeled with contributions from both charged-particle sputtering using a Sigmund-Thomson velocity distribution [*Sigmund*, 1969] and micrometeoroid impact vaporization with a temperature of 3000 K [*Eichhorn*, 1976]. We exclude ions produced directly from the surface via solar wind sputtering [i.e., *Elphic et al.*, 1991], in line with constraint (d) on the LDEX data discussed in section 3. He, Ne, and CO are modeled as thermally accommodated species, while for Ar, we adopt the spatial distribution from the model of *Grava et al.* [2015], which peaks near dawn and rapidly declines toward noon. Ionization rates for all neutral species are assumed to be from photoionization at solar median [*Huebner et al.*, 1992; *Huebner and Mukherjee*, 2015] with solar wind proton charge exchange also operating for Ar and CO [*Barnett and Reynolds*, 1958; *Cravens et al.*, 1987].

Figure 4a shows the ion production rates as a function of altitude for solar zenith angle equal to 45° for all species from the model as described above. In this model, Al^+ is predicted to be the dominant ion species with a production rate at the surface of ≈7000 cm^{-3} s^{-1}, followed by CO^+ and Ar^+ surface production rates of ≈1800 and ≈1250 cm^{-3} s^{-1}, respectively. All other species combined comprise approximately 15% of the total ion production rate. The observed NMS ion production rate between altitudes of 20 and 100 km [*Halekas et al.*, 2015] is denoted by the gray shaded region (with approximate error of a factor of 2). NMS observed all ions shown in Figure 4 except Mg^+, Al^+, Ti^+, and Fe^+ between 20 and 100 km. The model prediction for the total ion production rate measured by NMS is denoted by the black dashed line and agrees well with the NMS data.

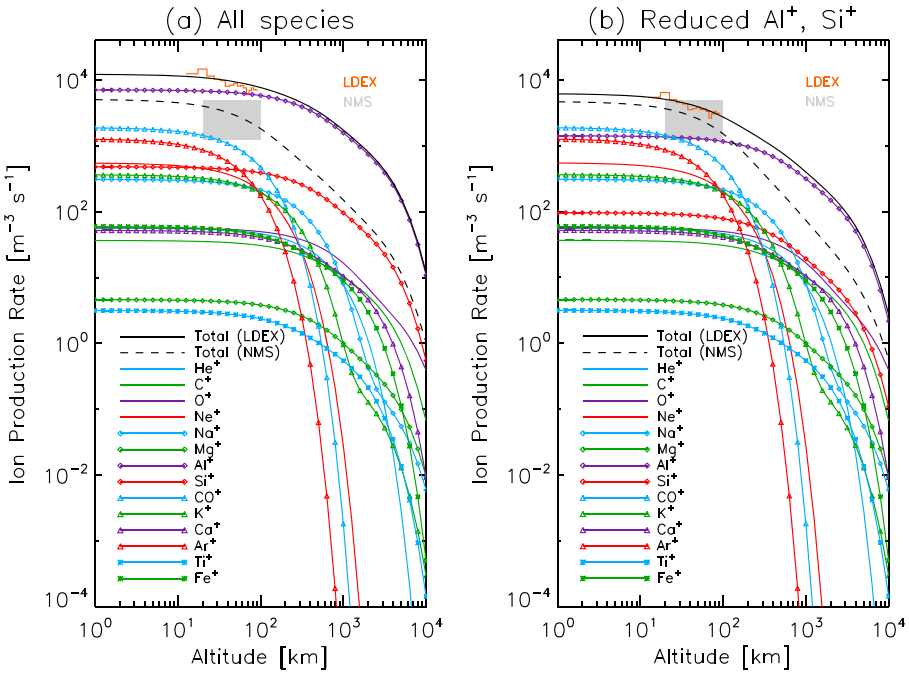

Figure 4. The modeled ion production rates at solar zenith angle of 45° for selected species based on the model of *Sarantos et al.* [2012a], LADEE/NMS neutral measurements of He/Ne/Ar reported by *Benna et al.* [2015], and LADEE/NMS ion mode measurements of C, O, and CO [*Halekas et al.*, 2015]. (a) The model for all species and (b) the model with reduced contributions from Al^+ and Si^+, as discussed in the text.

While the absolute calibration of the LDEX efficiency is uncertain and, thus, we cannot firmly establish the absolute ion production rate, we can compare the altitude dependence of the LDEX data to the model by normalizing the LDEX observations to match the sum of all individual ion production rates from the model since LDEX indiscriminately observes all pickup ions regardless of species. The median observed LDEX production rate is shown in orange as a function of altitude and compared to the modeled sum, shown as the solid black line. The model predicts that the LDEX current is dominated by Al^+ ions (≈60% of the total); however, the Al^+ scale height from the model, ≈400 km, is somewhat inconsistent with the LDEX observations which show a smaller scale height of ≈100 km.

In order to explore the possibility of a better fit, we reduce the modeled contribution of Al^+ and Si^+ ion production by 80% relative to that shown in Figure 4a, motivated by both the need to reduce the total scale height and taking into consideration that *Cook et al.* [2013] have published upper limits to neutral Al and Si densities of 1.1 and 0.9 cm^{-3}, respectively, a factor of several lower than that predicted by *Sarantos et al.* [2012a] of 6.6 and 23.3 cm^{-3}, respectively. Figure 4b shows the modeled ion production rates with reduced Al^+ and Si^+ contributions and comparisons to both NMS and LDEX. In this model, Al^+, CO^+, and Ar^+ each contribute roughly 25% of the total ion production rate (under an altitude of ≈100 km), with the remaining 25% consisting of all other species combined. The LDEX altitude profile matches very well to the total production rate in this case, with an effective scale height of ≈100 km. This fit suggests that Al^+, and potentially Si^+, contribute less to the ion production rate than predicted by the model of *Sarantos et al.* [2012a]. There are several sources of uncertainty in the neutral model of *Sarantos et al.* [2012a] for both micrometeorite impact vaporization and charged-particle sputtering, including the mass influx of micrometeoroids, the impact vaporization yield, and the absolute charged-particle sputtering yield of lunar regolith. Concurrent spectral measurements by the LADEE Ultraviolet Spectrometer [*Colaprete et al.*, 2014] could help to quantify the neutral densities of Al and Si in the lunar exosphere relative to the model of *Sarantos et al.* [2012a].

In addition to constraining models of the lunar pickup ion composition, the variations in the lunar pickup ion production rate tell us much about the structure and behavior of the lunar exosphere. The linear increase in ion volume production rate as a function of solar wind flux is best interpreted as a detection of the role that the solar wind plays in both generating and ionizing the lunar exosphere. Charged-particle sputtering of the lunar surface is a major source of refractory species in the exosphere [i.e., *Wurz et al.*, 2007; *Sarantos et al.*, 2012a],

and charge exchange rates for some neutral species such as Ar and CO are on the order of or larger than their respective photoionization rates [*Barnett and Reynolds*, 1958; *Cravens et al.*, 1987]. Despite the relatively low number of measurements, we also interpret the constant ion production rate at lower solar wind flux ($<10^8$ cm^{-2} s^{-1}) as evidence of other, well-known exospheric generation mechanisms uncorrelated with solar wind flux (i.e., micrometeoroid impact vaporization, thermal desorption, and photon-stimulated desorption). The variation of pickup ion production as a function of altitude is indicative of a neutral scale height (averaged over all species according to their ionization rates) of ≈100 km. This reflects the dominance of both Ar^+ and CO^+ as discussed above, with thermal scale heights of 49 and 70 km, respectively. Al^+, as a nonthermal species, may extend the pickup ion production to much higher altitudes as seen from the model in Figure 4, especially at times of high solar wind flux and/or heavy micrometeoroid bombardment, yet the LDEX data limit the overall contribution of Al^+ based on the observed scale height of the ion production rate. Finally, the local time dependence of the pickup ion production rate suggests a fairly isotropic ionization rate with some evidence of a local maximum near 07–08 LT. This trend agrees well with NMS ionization rate observations, which observed Ar^+ and mass 28 amu ions (presumably CO^+ as argued by *Halekas et al.* [2015]) with peaks just sunward of the dawn terminator near 07–08 LT with significant production extending toward noon.

5. Conclusion

We have reported serendipitous measurements of low-energy lunar pickup ions by the LADEE LDEX instrument during its 6 month prime mission in orbit around the Moon. Lunar exospheric pickup ion production was observed to have an approximate scale height of 100 km, to be linearly correlated with the solar wind flux to the lunar surface and to be relatively flat as a function of local time with some suggestion of a peak near 07–08 LT. Comparison to concurrent measurements of the lunar exosphere by the LADEE/NMS instrument [*Benna et al.*, 2015; *Halekas et al.*, 2015] and an exospheric model [*Sarantos et al.*, 2012a] finds good agreement, with the exception of Al^+ and possibly Si^+, which may be overestimated in the model. Indeed, *Cook et al.* [2013] reported an upper limit for the neutral Al density at dawn of 1.1 cm^{-3} using Lunar Reconnaissance Orbiter Lyman Alpha Mapping Project observations, a factor of approximately 6 lower than that of *Sarantos et al.* [2012a]. Continued determination of the density of all exospheric species, in particular Al, may help to resolve this disagreement. Additionally, a reanalysis of the ARTEMIS pickup ion measurements [e.g., *Halekas et al.*, 2012b] in light of the knowledge gained from the LADEE mission may prove insightful especially given that ARTEMIS has now collected more than 4 years of lunar pickup ion observations. Finally, we note that the results presented here have implications for the formation and ionization of neutral exospheres at airless bodies throughout the solar system, especially inner solar system asteroids [e.g., *Morgan and Killen*, 1998; *Schläppi et al.*, 2008; *Altwegg et al.*, 2012] and the moons of Mars [e.g., *Cipriani et al.*, 2011; *Poppe and Curry*, 2014].

Acknowledgments
A.R.P. and J.S.H. gratefully acknowledge support from both the NASA LADEE Guest Investigator program, grant #NNX13AO71G, and the NASA LASER program, grant #NNX13AJ97G. J.S., M.H., Z.L., and S.K. acknowledge support from the NASA's SSERVI IMPACT team. The authors also thank R.C. Elphic and G.T. Delory for their excellent work in leading the LADEE team and ensuring the success of the mission. The ARTEMIS mission is funded and operated under NASA grant #NAS5-02099, and we specifically acknowledge J.P. McFadden for the use of ESA data and K.-H. Glassmeier, U. Auster, and W. Baumjohann for the use of FGM data provided under the lead of the Technical University of Braunschweig and with financial support through the German Ministry for Economy and Technology and the German Center for Aviation and Space (DLR) under contract 50-OC-0302. ARTEMIS data are publicly available at http://artemis.ssl.berkeley.edu, and LADEE/LDEX data are available through NASA's Planetary Data System. Finally, the authors thank two reviewers for constructive comments.

References

Altwegg, K., et al. (2012), In situ mass spectrometry during the Lutetia flyby, *Planet. Space Sci.*, *66*, 173–178.
Barnett, C. F., and H. K. Reynolds (1958), Charge exchange cross sections of hydrogen particles in gases at high energies, *Phys. Rev.*, *109*(2), 355–359.
Benna, M., P. R. Mahaffy, J. S. Halekas, R. C. Elphic, and G. T. Delory (2015), Variability of helium, neon, and argon in the lunar exosphere as observed by the LADEE NMS instrument, *Geophys. Res. Lett.*, *42*, 3723–3729, doi:10.1002/2015GL064120.
Cipriani, F., O. Witasse, F. Leblanc, R. Modolo, and R. E. Johnson (2011), A model of interaction of Phobos' surface with the Martian environment, *Icarus*, *212*, 643–648.
Colaprete, A., K. Vargo, M. Shirley, D. Landis, D. Wooden, J. Karcz, B. Hermalyn, and A. Cook (2014), An overview of the LADEE ultraviolet-visible spectrometer, *Space Sci. Rev.*, *185*(1–4), 63–91.
Colaprete, A., M. Sarantos, D. H. Wooden, T. J. Stubbs, A. M. Cook, and M. Shirley (2016), How surface composition and meteoroid impacts mediate sodium and potassium in the lunar exosphere, *Science*, *351*(6270), 249–252.
Cook, J. C., S. A. Stern, P. D. Feldman, G. R. Gladstone, K. D. Retherford, and C. C. C. Tsang (2013), New upper limits on numerous atmospheric species in the native lunar atmosphere, *Icarus*, *225*, 681–687.
Cravens, T. E., J. U. Kozyra, A. F. Nagy, T. I. Gombosi, and M. Kurtz (1987), Electron impact ionization in the vicinity of comets, *J. Geophys. Res.*, *92*(A7), 7341–7353.
Eichhorn, G. (1976), Analysis of the hypervelocity impact process from impact flash measurements, *Planet. Space Sci.*, *24*, 771–781.
Elphic, R. C., H. O. Funsten III, B. L. Barraclough, D. J. McComas, M. T. Paffett, D. T. Vaniman, and G. Heiken (1991), Lunar surface composition and solar wind-induced secondary ion mass spectrometry, *Geophys. Res. Lett.*, *18*(11), 2165–2168.
Elphic, R. C., G. T. Delory, B. P. Hine, P. R. Mahaffy, M. Horányi, A. Colaprete, M. Benna, and S. K. Noble (2014), The Lunar Atmosphere and Dust Environment Explorer mission, *Space Sci. Rev.*, *185*, 3–26.
Grava, C., J.-Y. Chaufray, K. D. Retherford, G. R. Gladstone, T. K. Greathouse, D. M. Hurley, R. R. Hodges, A. J. Bayless, J. C. Cook, and S. A. Stern (2015), Lunar exospheric argon modeling, *Icarus*, *255*, 135–147.
Halekas, J. S., A. R. Poppe, G. T. Delory, M. Sarantos, W. M. Farrell, V. Angelopoulos, and J. P. McFadden (2012a), Lunar pickup ions observed by ARTEMIS: Spatial and temporal distribution and constraints on species and source locations, *J. Geophys. Res.*, *117*, E06006, doi:10.1029/2012JE004107.

Halekas, J. S., et al. (2012b), Lunar precursor effects in the solar wind and terrestrial magnetosphere, *J. Geophys. Res.*, *117*, A05101, doi:10.1029/2011JA017289.
Halekas, J. S., A. R. Poppe, J. P. McFadden, and K.-H. Glassmeier (2013), The effects of reflected protons on the plasma environment of the Moon for parallel interplanetary magnetic fields, *Geophys. Res. Lett.*, *40*, 4544–4548, doi:10.1002/grl.50892.
Halekas, J. S., M. Benna, P. R. Mahaffy, R. C. Elphic, A. R. Poppe, and G. T. Delory (2015), Detections of lunar exospheric ions by the LADEE neutral mass spectrometer, *Geophys. Res. Lett.*, *42*, 5162–5169, doi:10.1002/2015GL064746.
Hartle, R. E., and R. Killen (2006), Measuring pickup ions to characterize the surfaces and exospheres of planetary bodies: Applications to the Moon, *Geophys. Res. Lett.*, *33*, L05201, doi:10.1029/2005GL024520.
Hilchenbach, M., D. Hovestadt, B. Klecker, and E. Möbius (1993), Observations of energetic lunar pick-up ions near Earth, *Adv. Space Res.*, *13*(10), 321–324.
Hodges, R. R., and P. R. Mahaffy (2016), Synodic and semiannual oscillations of argon-40 in the lunar exosphere, *Geophys. Res. Lett.*, *43*, 22–27, doi:10.1002/2015GL067293.
Horányi, M., et al. (2014), The Lunar Dust Experiment (LDEX) Onboard the Lunar Atmosphere and Dust Environment Explorer (LADEE) Mission, *Space Sci. Rev.*, *185*, 93–114.
Huebner, W. F., and J. Mukherjee (2015), Photoionization and photodissociation rates in solar and blackbody radiation fields, *Planet. Space Sci.*, *106*, 11–45.
Huebner, W. F., J. J. Keady, and S. P. Lyon (1992), Solar photo rates for planetary atmospheres and atmospheric pollutants, *Astrophys. Space Sci.*, *195*, 1–294.
Hurley, D. M., et al. (2016), Understanding temporal and spatial variability of the lunar helium atmosphere using simultaneous observations from LRO, LADEE, and ARTEMIS, *Icarus*, doi:10.1016/j.icarus.2015.09.011, in press.
Lue, C., Y. Futaana, S. Barabash, M. Wieser, M. Holmström, A. Bhardwaj, M. B. Dhanya, and P. Wurz (2011), Strong influence of lunar crustal fields on the solar wind flow, *Geophys. Res. Lett.*, *38*, L03202, doi:10.1029/2010GL046215.
Mahaffy, P. R., et al. (2014), The Neutral Mass Spectrometer on the Lunar Atmosphere and Dust Environment Explorer, *Space Sci. Rev.*, *185*, 27–62.
Mall, U., E. Kirsch, K. Cierpka, B. Wilken, A. Söding, F. Neubauer, G. Gloeckler, and A. B. Galvin (1998), Direct observation of lunar pick-up ions near the Moon, *Geophys. Res. Lett.*, *25*(20), 3799–3802.
Morgan, T. H., and R. M. Killen (1998), Production mechanisms for faint by possibly detectable coronae about asteroids, *Planet. Space Sci.*, *46*(8), 843–850.
Poppe, A. R., and S. M. Curry (2014), Martian planetary heavy ion sputtering of Phobos, *Geophys. Res. Lett.*, *41*, 6335–6341, doi:10.1002/2014GL061100.
Poppe, A. R., R. Samad, J. S. Halekas, M. Sarantos, G. T. Delory, W. M. Farrell, V. Angelopoulos, and J. P. McFadden (2012), ARTEMIS observations of lunar pick-up ions in the terrestrial magnetotail, *Geophys. Res. Lett.*, *39*, L17104, doi:10.1029/2012GL052909.
Rodríguez, D. F., L. Saul, P. Wurz, S. A. Fuselier, H. O. Funsten, D. J. McComas, and E. Möbius (2012), IBEX-Lo observations of energetic neutral hydrogen atoms originating from the lunar surface, *Planet. Space Sci.*, *60*, 297–303.
Saito, Y., et al. (2008), Solar wind proton reflection at the lunar surface: Low energy ion measurement by MAP-PACE onboard SELENE (KAGUYA), *Geophys. Res. Lett.*, *35*, L24205, doi:10.1029/2008GL036077.
Sarantos, M., R. M. Killen, D. A. Glenar, M. Benna, and T. J. Stubbs (2012a), Metallic species, oxygen and silicon in the lunar exosphere: Upper limits and prospects for LADEE measurements, *J. Geophys. Res.*, *117*, A03103, doi:10.1029/2011JA017044.
Sarantos, M., R. E. Hartle, R. M. Killen, Y. Saito, J. A. Slavin, and A. Glocer (2012b), Flux estimates of ions from the lunar exosphere, *Geophys. Res. Lett.*, *39*, L13101, doi:10.1029/2012GL052001.
Schläppi, B., K. Altwegg, and P. Wurz (2008), Asteroid exosphere: A simulation for the ROSETTA flyby targets (2867) Steins and (21) Lutetia, *Icarus*, *195*, 674–685.
Sigmund, P. (1969), Theory of sputtering. I. Sputtering yield of amorphous and polycrystalline targets, *Phys. Rev.*, *184*, 383–416.
Stern, S. A. (1999), The lunar atmosphere: History, status, current problems, and context, *Rev. Geophys.*, *37*(4), 453–491.
Szalay, J. R., and M. Horányi (2015), The search for electrostatically lofted grains above the Moon with the Lunar Dust Experiment, *Geophys. Res. Lett.*, *42*, 5141–5146, doi:10.1002/2015GL064324.
Tanaka, T., et al. (2009), First in situ observation of the Moon-originating ions in the Earth's Magnetosphere by MAP-PACE on SELENE (KAGUYA), *Geophys. Res. Lett.*, *36*, L22106, doi:10.1029/2009GL040682.
Vorburger, A., P. Wurz, S. Barabash, M. Wieser, Y. Futaana, M. Holmström, A. Bhardwaj, and K. Asamura (2014), First direct observation of sputtered lunar oxygen, *J. Geophys. Res. Space Physics*, *119*, 709–722, doi:10.1002/2013JA019207.
Walker, J., J. S. Halekas, A. R. Poppe, J. R. Szalay, and M. Horányi (2015), Measurement of energetic neutral atom flux in the lunar exosphere using the LDEX instrument, Abstracts SM31B-2497 presented at 2015 Fall Meeting, AGU, San Francisco, Calif., 14–18 Dec.
Wieser, M., S. Barabash, Y. Futaana, M. Holmström, A. Bhardwaj, R. Sridharan, M. B. Dhanya, P. Wurz, A. Schaufelberger, and K. Asamura (2009), Extremely high reflection of solar wind protons as neutral hydrogen atoms from regolith in space, *Planet. Space Sci.*, *57*, 2132–2134.
Wurz, P., U. Rohner, J. A. Whitby, C. Kolb, H. Lammer, P. Dobnikar, and J. A. Martín-Fernández (2007), The lunar exosphere: The sputtering contribution, *Icarus*, *191*, 486–496.
Yakshinskiy, B. V., and T. E. Madey (1999), Photon-stimulated desorption as a substantial source of sodium in the lunar atmosphere, *Nature*, *400*, 642–644.
Yakshinskiy, B. V., and T. E. Madey (2004), Photon-stimulated desorption of Na from a lunar sample: Temperature-dependent effects, *Icarus*, *168*, 53–59.
Yokota, S., et al. (2009), First direct detection of ions originating from the Moon by MAP-PACE IMA onboard SELENE (KAGUYA), *Geophys. Res. Lett.*, *36*, L11201, doi:10.1029/2009GL038185.